Basic Res Cardiol (2010) 105:465–477
DOI 10.1007/s00395-010-0090-7

ORIGINAL CONTRIBUTION

CB_1 receptor inhibition leads to decreased vascular AT1 receptor expression, inhibition of oxidative stress and improved endothelial function

Vedat Tiyerili · Sebastian Zimmer · Suzin Jung · Kerstin Wassmann · Claas P. Naehle · Dieter Lütjohann · Andreas Zimmer · Georg Nickenig · Sven Wassmann

Received: 17 December 2009 / Revised: 3 February 2010 / Accepted: 4 February 2010 / Published online: 2 April 2010
© Springer-Verlag 2010

Abstract Inhibition of the cannabinoid receptor CB_1 (CB_1-R) exerts numerous positive cardiovascular effects such as modulation of blood pressure, insulin sensitivity and serum lipid concentrations. However, direct vascular effects of CB_1-R inhibition remain unclear. CB_1-R expression was validated in vascular smooth muscle cells (VSMCs) and aortic tissue of mice. Apolipoprotein E-deficient (ApoE−/−) mice were treated with cholesterol-rich diet and the selective CB_1-R antagonist rimonabant or vehicle for 7 weeks. CB_1-R inhibition had no effect on atherosclerotic plaque development, collagen content and macrophage infiltration but led to improved aortic endothelium-dependent vasodilation and decreased aortic reactive oxygen species (ROS) production and NADPH oxidase activity. Treatment of cultured VSMC with rimonabant resulted in reduced angiotensin II-mediated but not basal ROS production and NADPH oxidase activity. CB_1-R inhibition with rimonabant and AM251 led to down-regulation of angiotensin II type 1 receptor (AT1-R) expression, whereas stimulation with the CB_1-R agonist CP 55,940 resulted in AT1-R up-regulation, indicating that AT1-R expression is directly regulated by the CB_1-R. CB_2-R inhibition had no impact on AT1-R expression in VSMC. Consistently, CB_1-R inhibition decreased aortic AT1-R expression in vivo. CB_1-R inhibition leads to decreased vascular AT1-R expression, NADPH oxidase activity and ROS production in vitro and in vivo. This antioxidative effect is associated with improved endothelial function in ApoE−/− mice, indicating beneficial direct vascular effects of CB_1-R inhibition.

Keywords Rimonabant · AT1 receptor · CB_1 receptor · Oxidative stress · Endothelial function

Introduction

The endocannabinoid system is composed of G-coupled protein cannabinoid receptors (CB_1, CB_2), endogenous ligands (endocannabinoids) and enzymes for ligand biosynthesis and inactivation [9, 27, 28]. The CB_1 receptor (CB_1-R) is mainly localized in the central nervous system but is also abundant in peripheral tissues including liver, skeletal muscle, myocardium, endothelial cells, gastrointestinal tract and adipose tissue [2, 3, 8]. The CB_2 receptor, on the other hand, is primarily expressed in cells of the immune system and endothelial cells [23, 49]. Activation of these receptors (CB_1, CB_2) has numerous important central and peripheral effects including modulation of blood pressure, heart rate, insulin sensitivity and serum lipid concentration, and may therefore be important for the development of atherosclerosis [15, 23, 42]. In fact,

V. Tiyerili and S. Zimmer contributed equally to this study.

V. Tiyerili · S. Zimmer · S. Jung · K. Wassmann · G. Nickenig · S. Wassmann (✉)
Medizinische Klinik und Poliklinik II, Universitätsklinikum Bonn, Sigmund-Freud-Str. 25, 53105 Bonn, Germany
e-mail: sven.wassmann@uni-bonn.de; sven.wassmann@mcgill.ca

C. P. Naehle
Radiologische Klinik, Universitätsklinikum Bonn, Bonn, Germany

D. Lütjohann
Institut für Klinische Chemie und Pharmakologie, Universitätsklinikum Bonn, Bonn, Germany

A. Zimmer
Institut für Molekulare Psychiatrie, Universitätsklinikum Bonn, Bonn, Germany

stimulation of the CB_2 receptor via low dose oral cannabinoid therapy reduces progression of atherosclerosis in mice [43].

Rimonabant is a selective, centrally active CB_1-R antagonist [15, 36]. It suppresses eating behavior and controls food intake by inhibiting the over-activity of the endocannabinoid system in adipose animals [6, 36]. In recent clinical trials, treatment of overweight patients with rimonabant resulted in significant weight loss and improvement of multiple cardio-metabolic risk factors, such as waist circumference, systolic blood pressure, HDL-cholesterol, triglyceride levels and insulin sensitivity [11, 35, 39, 48]. The underlying mechanisms promoting these beneficial cardio-metabolic effects of CB_1-R inhibition, however, remain unclear and have stimulated significant scientific interest. Focus of the recent STRADIVARIUS study was to evaluate the effect of rimonabant treatment in patients with abdominal obesity and coronary artery disease on the progression of atherosclerosis [32]. Consistent with the RIO trials, rimonabant treatment led to improved cardiovascular risk factors but was inconclusive with respect to atherogenesis. The primary endpoint (percent atheroma volume) did not reach statistical significance but the secondary efficacy parameter (total atheroma volume) showed a significant improvement in patients treated with rimonabant [32].

A growing body of evidence suggests that the endocannabinoid system plays a critical role in the pathogenesis of atherosclerosis [24, 27, 44]. It modulates clinical and preclinical manifestations, such as oxidative stress, endothelial dysfunction, ischemic heart disease and cerebrovascular disease [25, 38]. However, the precise role of the endocannabinoid system and especially the CB_1-R in the vascular system and atherosclerosis are not fully understood. We have now investigated the effects of CB_1-R inhibition on cardio-metabolic risk factors, oxidative stress, endothelial function and atherogenesis in a mouse model of atherosclerosis and examined the underlying molecular mechanisms in cell culture experiments.

Methods

Materials

Lucigenin, oil red O solution, salts, and other chemicals were purchased from Sigma Chemical. L-012 was obtained from Wako Chemicals. MMLV reverse transcriptase, antibiotics, fetal calf serum, and cell culture medium were acquired from Invitrogen. AM251 was purchased from Cayman Chemical and CP 55,940 from BioTrend. Rimonabant and SR 144528 were provided by Sanofi-Aventis. The L15 (CB_1-R) antibody was a kind gift from Ken Mackie (Indiana, USA).

Cell culture

Vascular smooth muscle cells (VSMCs) were isolated from rat (Sprague Dawley) and mouse (C57BL/6J) thoracic aortas and were cultured over several passages. Experiments were performed with cells from passages 5 to 8. Stimulation of VSMCs was conducted with angiotensin II (10^{-6} M) for 3 h, and rimonabant (10^{-6}/10^{-7} M), AM251 (10^{-6} M), CP 55,940 (10^{-6} M) and SR 144528 (10^{-6} M) for 24 h. Rimonabant was dissolved in 0.1% Tween 80 (AppliChem) for in vivo studies. For cell culture experiments, rimonabant, CP 55,940 and SR 144528 were dissolved in DMSO.

Animals and procedures

Female, 12-week and 9-month-old apolipoprotein E-deficient (ApoE−/−) mice (C57BL/6J genetic background from Charles River) were used for this study. Tissue from CB_1-R [58] and CB_2-R [4] knockout mice was used for corresponding negative mRNA and protein controls. For positive mRNA and protein controls, tissue from wild-type C57BL/6J mice was used. The animals were maintained in a 22°C room with a 12-h light/dark cycle. ApoE−/− mice were fed a high-fat, cholesterol-rich diet for 7 weeks that contained 21% fat, 19.5% casein, and 1.25% cholesterol (Ssniff, Germany) and were concomitantly treated with vehicle or rimonabant (10 mg/kg body weight/day) via drinking water [36]. Plasma cholesterol concentrations were determined by gas–liquid chromatography–mass spectrometry. Body weights were measured weekly. Arterial blood pressure was assessed with a computerized tail-cuff method (CODA 6, Kent Scientific) before and after treatment. Abdominal fatty tissue was only analyzed in 9-month-old ApoE−/− mice. The mice were killed after the treatment period, and tissue samples and blood were collected immediately. All animal experiments were performed in accordance with institutional guidelines and the German animal protection law.

Aortic ring preparations and tension recording

Vasodilation and vasoconstriction of isolated aortic ring preparations were determined in organ baths filled with oxygenated modified Tyrode buffer, as previously described [51, 54].

Staining of atherosclerotic lesions and histological analysis

Hearts with ascending aortas were embedded in Tissue Tek OCT embedding medium and sectioned on a Leica cryostat (9 µm), starting at the apex and progressing

through the aortic valve area into the ascending aorta and the aortic arch. For the detection of atherosclerotic lesions, aortic cryosections were fixed with 3.7% formaldehyde and stained with oil red O working solution. For immunohistochemical analysis, cryosections placed on poly-L-lysine (Sigma)-coated slides were assessed for the macrophage marker MOMA-2 with an indirect immunoenzymatic method. Slides were incubated with acetone for 30 min at −20°C. Then, PBS-washed slides were preincubated with 10% normal goat serum (Sigma) for 30 min. The primary antibody (monoclonal rat anti-mouse MOMA-2 antibody, Acris) was applied for 1 h at room temperature and thereafter at 4°C overnight. Slides were then incubated with an alkaline phosphatase-conjugated secondary antibody (goat anti-rat IgG, Sigma) for 1 h at room temperature. Color reaction was accomplished with FastRed (Sigma) as a chromogenic substrate. Nuclei were counterstained with hematoxylin. Isotype-specific antibodies were used for negative controls. Sections were washed and mounted with Aquatex mounting medium (Sigma) for light microscopic analysis. All sections were examined under a Zeiss Axiovert 200M microscope using AxioVision version 4.5.0 software. For quantification of atherosclerotic plaque formation in the aortic root, lipid-staining area and total area of serial histological sections were measured. Atherosclerosis data are expressed as lipid-staining area in percent of total surface area. The investigators who performed the histological analyses were blinded to the treatment of the respective animal group.

Measurement of reactive oxygen species (ROS)

Reactive oxygen species release in intact aortic segments was determined by L-012 chemiluminescence, as previously described [52]. Intracellular ROS production in VSMCs was measured by 2′,7′-dichlorofluorescein (DCF; 10 μmol/l) fluorescence microscopy, as described previously [53]. The relative fluorescence intensity is the average value of all experiments.

Measurement of NADPH oxidase activity

Measurement of NADPH oxidase activity was measured by a lucigenin-enhanced chemiluminescence assay, as previously described [1]. Aortic tissue was mechanically lysed using a glass/Teflon potter and cell cultures were lysed using a Sonorex (Bandelin) in ice-cold buffer B lacking lucigenin and substrate. Total protein concentration was adjusted to 1 mg/ml. Aliquots of the protein sample (100 μl) were measured over 10 min in quadruplicates using NADPH as substrate in a scintillation counter (Berthold Lumat LB 9501) in 1-min intervals.

Western blotting

After treatment, VSMCs and aortas, respectively, were homogenized in ice-cold lysis buffer containing additional leupeptin and aprotinin. Protein aliquots were separated on SDS/PAGE. Western blotting of proteins was performed in a semidry blotting chamber (Pharmacia Biotech) and incubated in 5% non-fat dry milk at 4°C overnight. Blot membranes were stained with Ponceau red to verify appropriate protein transfer and equal loading for each lane. Immunoblotting was performed with an AT1 receptor rabbit polyclonal IgG antibody (1:500 dilution, sc 1173, AT1 (N-10), Santa Cruz Biotechnology), the L15 CB_1-R rabbit antibody (1:500 dilution, Mackie Lab, Indiana, USA) or the CB_2-R polyclonal rabbit antibody (1:1,000 dilution, ab3561, Abcam) for 60 min at 37°C. Immunodetection was accomplished using a goat anti-rabbit secondary antibody (1:5,000 dilutions, Sigma Chemical) and the enhanced chemiluminescence kit (Amersham). Membranes were stripped with Roti-Free (Carl Roth, Germany) at 56°C for 20 min and then incubated with anti-GAPDH monoclonal mouse antibody (1:3,000 dilution, Cat 5G4 MAb 6C5, HyTest) for 12 h at 4°C. Immunodetection was performed with a goat anti-mouse IgG secondary antibody (peroxidase antibody, 1:4,000 dilution, A5278, Sigma Chemical). Brain tissue of wild-type and CB_1-R−/− mice was used for positive and negative controls in all CB_1-R Western blots. For positive and negative controls of CB_2-R expression, spleens of wild-type and CB_2-R−/− mice were used. No CB_1-R or CB_2-R signal was detected in the corresponding knockout controls.

Real-time polymerase chain reaction

For the assessment of vascular gene expression, mouse aortas were excised, quickly frozen in liquid nitrogen, and homogenized with a motorized homogenizer. For analysis of gene expression in cultured VSMCs, cells were lysed using a 10 G needle and homogenized with a motorized homogenizer. RNA was isolated with peqGOLD RNA-Pure (peqLAB Biotechnology). RNA concentration and quality was verified with a spectrophotometer. Then, 1 μg of the isolated total RNA was reverse transcribed using random primers and MMLV reverse transcriptase (Invitrogen) for 60 min at 42°C and 10 min at 75°C. The single-stranded cDNA was amplified by real-time quantitative reverse transcription-polymerase chain reaction (RT-PCR) with the TaqMan system (ABI-7500 fast PCR System) using SYBR-Green dye. For AT1 receptor, the primers 5′-GGG TGG ACA ATG GCC AGG TAG-3′ and 5′-CTC GCC CTG GCT GAC TTA TGC-3′ were used. For 18s rRNA, the primers 5′-TTG ATT AAG TCC CTG CCC TTT GT-3′ and 5′-CGA TCC GAG GGC CTC ACT A-3′

were used. For quantification, AT1 receptor mRNA expression was normalized to endogenous 18s rRNA according to previously published protocols [26].

For CB_1-R and CB_2-R RT-PCR, commercially available Taqman® probes were used (Applied Biosystems) and implemented according to the manufacturer's protocols. CB_1-R and CB_2-R mRNA expression was normalized to GAPDH (Taqman® probes, Applied Biosystems). Brain tissue of wild-type and CB_1-R−/− mice was used for positive and negative controls, respectively. For positive and negative controls of CB_2-R expression, spleens of wild-type and CB_2-R−/− mice were used. No CB_1-R or CB_2-R signal was detected in the corresponding knockout controls.

Glucose and insulin tolerance test

Twelve-week-old and 9-month-old ApoE−/− mice were used to analyze insulin sensitivity. Glucose and insulin tolerance tests were conducted after treatment with rimonabant or vehicle. In order to determine blood glucose levels, an intraperitoneal glucose tolerance test (ipGTT) was executed. The mice were refrained from eating for 18 h and given glucose (G 20 Glucose solution, B. Braun) adjusted to their body weight (2 g/kg body weight) by intraperitoneal injection after a blood sample was collected from the tail vein. Blood glucose readings were taken after 15, 30, 60, 90 and 120 min. The Ascensia ELITE blood glucose monitoring system (Bayer) using the sip-in technology was applied for all measurements. In addition, an intraperitoneal insulin tolerance test (ipITT) was executed after 6-h fasting. Here, the animals were injected human insulin (Actrapid; Novo-Nordisk; 0.75 U/kg body weight) intraperitoneally after a blood sample was collected from the tail vein. Blood glucose readings were taken after 15, 30, 60, 90 and 120 min.

Computed tomography (CT) scans

Computed tomography scans were used for the quantification of abdominal visceral fatty tissue in mice. Before scanning, the animals were anesthetized with 75 mg/kg body weight ketaminehydrochloride (Ketanest, Pharmacia) and 5 mg/kg body weight xylazinehydrochloride (Rompun 2%, Bayer). The mice were placed in rigid PVC tubes to assure adequate separation and minimal movement. All CT scans were performed with a 64-detector CT scanner (Brilliance 64, Philips Medical Systems, Best, The Netherlands). Sequential CT scans were obtained with a tube current of 240 mA and a peak tube voltage of 120 kV. The scanning direction was craniocaudal, and the entire mouse was covered by the scan volume. The following CT scanning parameters were used for image acquisition: step-and-shoot axial scanning direction without overlap, 64 × 0.625-mm collimation, 0.5-s 360° gantry rotation time, field-of-view 194 mm, matrix 768 × 768 pixels, in-plane resolution 0.26 × 0.26 mm. The automated quantification of the abdominal visceral fat distribution was performed using Adobe Photoshop CS3 software (Adobe Systems). Best depiction ratios of abdominal fat areas were established at the CT abdominal level ($W = 350$; $L = 60$). "Fatty tissue pixels" were selected according to their luminance on a calibrated scale equivalent to 50–100 HU (Hounsfield units). This number was expressed as a ratio to the total number of pixels (the cross-sectional area of one mouse). 20 slices per mouse were analyzed.

Statistical analysis

Data are presented as mean ± standard error of mean (SEM). For statistical analysis, two-tailed, unpaired Student's t test and ANOVA for multiple comparisons were employed where applicable. $p < 0.05$ indicates statistical significance.

Results

CB_1 receptor expression

It has been reported that the cannabinoid receptors CB_1 and CB_2 are expressed in cardiovascular cells, including endothelial cells, the myocardium, adipose tissue and cells of the immune system [34]. We have confirmed, by real-time RT-PCR and Western analysis, that the CB_1-R is expressed in cultured rat aortic VSMCs (Fig. 1a) and aortic tissue of ApoE−/− mice (Fig. 1b) and in cultured mouse aortic VSMCs and aortic tissue of wild-type mice (data not shown). Stimulation or inhibition of a receptor may regulate its expression. We, therefore, analyzed the effects of CB_1-R inhibition on CB_1-R expression. First, VSMCs were incubated with rimonabant for 24 h, and CB_1-R protein and mRNA expression were then measured from cell lysates. Rimonabant incubation did not significantly change CB_1-R expression (protein: 100 ± 22% of control for vehicle vs. 94 ± 11% of control for rimonabant, Fig. 1a, left; mRNA: $1.00 \pm 0.03\ 2^{-\Delta\Delta Ct}$ for vehicle vs. $0.89 \pm 0.11\ 2^{-\Delta\Delta Ct}$ for rimonabant, Fig. 1a, right). Next, we studied CB_1-R expression in aortic tissue of ApoE−/− mice that received cholesterol-rich diet and rimonabant or vehicle for 7 weeks. Consistent with the in vitro findings, CB_1-R expression was also not significantly affected in vivo (protein: 100 ± 32% of control for vehicle vs. 87 ± 16% of control for rimonabant, Fig. 1b, left; mRNA: $1.00 \pm 0.15\ 2^{-\Delta\Delta Ct}$ for vehicle vs. $0.68 \pm 0.12\ 2^{-\Delta\Delta Ct}$ for rimonabant, Fig. 1b, right).

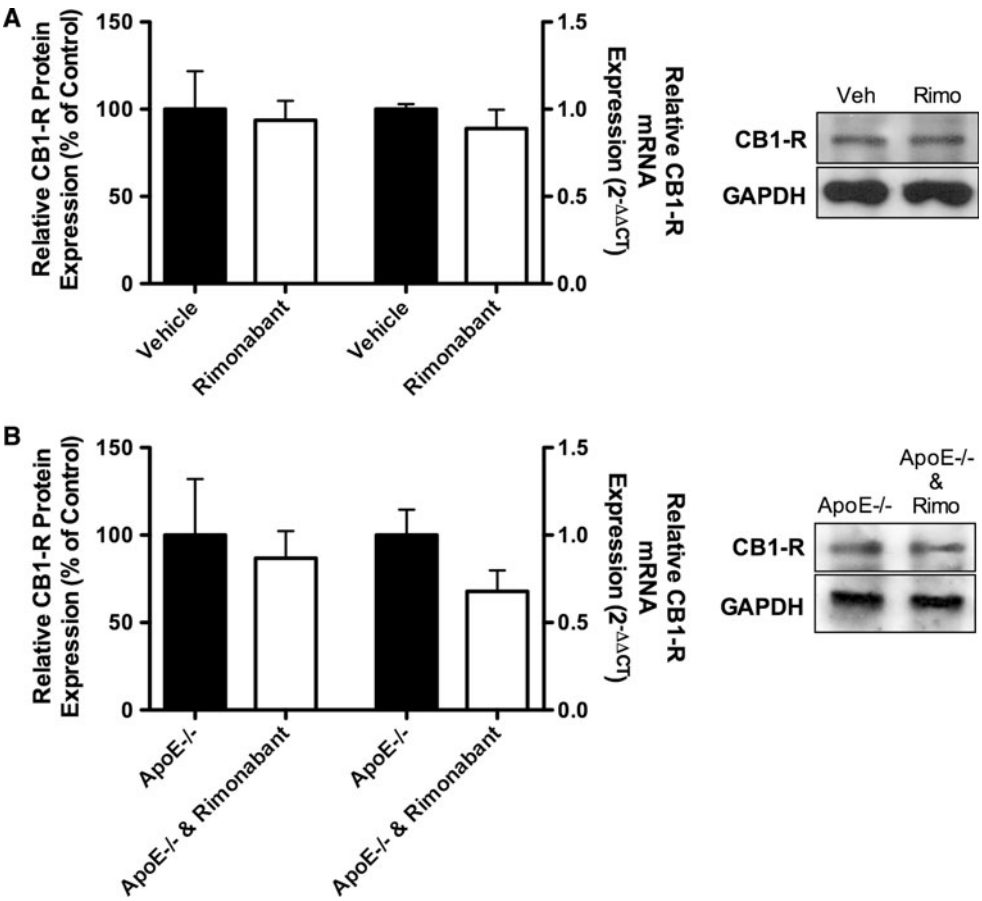

Fig. 1 **a** CB_1-R protein and mRNA expression in cultured rat aortic VSMCs after 24-h incubation with vehicle or rimonabant. Mean ± SEM, $n = 5$–6. **b** Aortic CB_1-R expression in ApoE−/− mice after a cholesterol-rich diet and treatment with either vehicle or rimonabant for 7 weeks. Mean ± SEM, $n = 5$. Quantitative protein analysis (*left*) with representative blot and relative change in mRNA (*right*)

Cardio-metabolic effects of rimonabant treatment

To analyze the vascular in vivo effects of CB_1-R inhibition, we fed 12-week-old ApoE−/− mice a high-fat, cholesterol-rich diet for 7 weeks and concomitantly treated them with the CB_1-R antagonist rimonabant (10 mg/kg body - weight/day) or vehicle via drinking water. Subsequently, we measured the cardio-metabolic parameters body weight, serum cholesterol, blood pressure, abdominal fatty tissue and glucose/insulin tolerance. Body weight was identical in both groups before treatment and only slightly but equally increased during the 7 weeks of cholesterol-rich diet (Table 1). There was no significant difference in serum cholesterol levels between the groups (Table 1). Systolic and diastolic blood pressure, as assessed by computerized tail-cuff method, remained unchanged before and after treatment (Table 1). The glucose and insulin tolerance tests showed no difference in 12-week-old ApoE−/− mice that were fed a cholesterol- and fat-rich diet and treated with rimonabant or vehicle for 7 weeks (data not shown). Because ApoE−/− mice develop insulin resistance and glucose intolerance with older age, we next treated 9-month-old ApoE−/− mice with the same diet and rimonabant concentrations. In the insulin tolerance test,

Table 1 Cardio-metabolic effects of rimonabant in ApoE−/− mice

	Vehicle	Rimonabants
Body weight (g)	24.7 ± 0.5	24.2 ± 0.5
Total cholesterol (mg/dl)	1,505 ± 65	1,554 ± 88
Systolic/diastolic blood pressure (mmHg)	124/93 ± 1/2	125/89 ± 2/3
Abdominal fatty tissue (% area)	21.6 ± 1.2	17.0 ± 0.9 *

ApoE−/− mice were fed a cholesterol-rich diet for 7 weeks and were concomitantly treated with vehicle or rimonabant. To determine cardio-metabolic effects, body weight, serum cholesterol concentrations, systolic and diastolic blood pressure and abdominal fatty tissue was assessed. Mean ± SEM, $n = 10$

*$p < 0.05$ versus vehicle

ApoE−/− mice treated with rimonabant became significantly more hypoglycemic 120 min after insulin injection (Fig. 2a). We also found a significant difference in the glucose tolerance test after 15 and 30 min (Fig. 2b), in favor of rimonabant-treated mice. Area under the curve (AUC) analyses confirmed the results of individual time points. Rimonabant treatment improved insulin sensitivity and glucose tolerance (ipITT: 261 ± 34 mg min/dl for vehicle vs. 161 ± 12 mg min/dl for rimonabant; ipGTT:

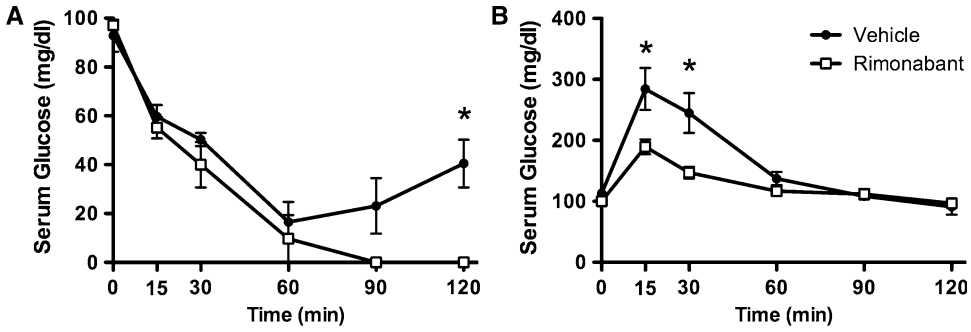

Fig. 2 Intraperitoneal glucose (**a**) and insulin tolerance tests (**b**) (ipITT and ipGTT) were conducted after treatment with rimonabant or vehicle in 9-month-old ApoE−/− mice that were concomitantly fed a high-fat, cholesterol-rich diet for 7 weeks. Mean ± SEM, $n = 10$, $^*p < 0.05$ versus vehicle

909 ± 88 mg min/dl for vehicle vs. 685 ± 35 mg min/dl for rimonabant). To quantify abdominal fatty tissue, CT scans of the 9-month-old ApoE−/− mice were conducted. Mice treated with rimonabant displayed significantly less abdominal fatty tissue compared to controls (Table 1).

Endothelial function

Next, we investigated endothelial function of intact isolated aortic ring preparations in organ chamber experiments. As shown in Fig. 3a, ApoE−/− mice developed endothelial dysfunction after 7 weeks of cholesterol-rich diet. Concomitant CB_1-R inhibition, however, significantly improved endothelium-dependent, carbachol-exerted vasodilation. Endothelium-independent vasodilation, as measured by nitroglycerin-induced vasorelaxation, was not significantly affected by the CB_1-R antagonist. Furthermore, rimonabant did not modulate phenylephrine or KCl-induced vasoconstriction (data not shown).

Atherosclerotic lesions

Atherosclerotic plaque formation (oil red O staining), collagen content (van Gieson) and macrophage infiltration (MOMA-2) of plaques were quantified after 7 weeks of cholesterol-rich diet in the aortic root and ascending aorta. Figure 3b shows representative cross-sections of the aortic root of both groups with atherosclerotic plaques. Cross-sectional lesion area analysis showed no significant difference between the groups (27.2 ± 3.5% plaque area for vehicle vs. 26.1 ± 2.3% plaque area for rimonabant, Fig. 3c). Furthermore, no significant difference was detected in collagen content and macrophage infiltration of the plaques (Fig. 3b).

Oxidative stress in vivo

An important cause of endothelial dysfunction is vascular oxidative stress, and the NADPH oxidase is a major source of ROS in the vessel wall [30, 31]. The improved endothelial function after rimonabant treatment could, therefore, be mediated by reduced NADPH oxidase-caused production of ROS. We assessed vascular ROS formation and NADPH oxidase activity in isolated aortic segments after the indicated treatments. CB_1-R inhibition with rimonabant significantly decreased ROS production in the vessel wall (vehicle: 100 ± 8% of control vs. rimonabant: 64 ± 9% of control, $p < 0.05$, Fig. 4a). In addition, NADPH oxidase activity was significantly reduced in aortas of rimonabant-treated mice (67 ± 7% of control, $p < 0.05$ vs. vehicle, Fig. 4b).

Oxidative stress in vitro

To further investigate the mechanisms by which in vivo CB_1-R inhibition improves endothelial function and decreases vascular oxidative stress, we next examined the effects of CB_1-R inhibition in vitro. Cultured VSMCs were incubated with the CB_1-R antagonist rimonabant and/or angiotensin II, and intracellular ROS production was measured by DCF fluorescence microscopy. As expected, stimulation with angiotensin II led to a significant increase in ROS production (137 ± 8% of control, $p < 0.05$ vs. vehicle, Fig. 4c). Incubation with rimonabant (10^{-6} M) alone did not affect basal cellular ROS formation (92 ± 9% of control), but CB_1-R inhibition significantly inhibited angiotensin II-mediated ROS production (98 ± 9% of control, $p < 0.05$ vs. angiotensin II). Consistently, the angiotensin II-induced increase in NADPH oxidase activity was inhibited by rimonabant in VSMCs (146 ± 43% of control vs. 44 ± 7% of control, $p < 0.05$, Fig. 4d).

CB_1 receptor inhibition and AT1 receptor expression

Because rimonabant inhibited angiotensin II-induced but not basal ROS production, and angiotensin II activates the NADPH oxidase through angiotensin II type 1 receptor (AT1-R) stimulation, we analyzed AT1-R expression in rat aortic VSMC. Similar to the effect of angiotensin II incubation, CB_1-R inhibition led to a significant down-regulation of AT1-R protein expression (Ang II: 24 ± 4% of

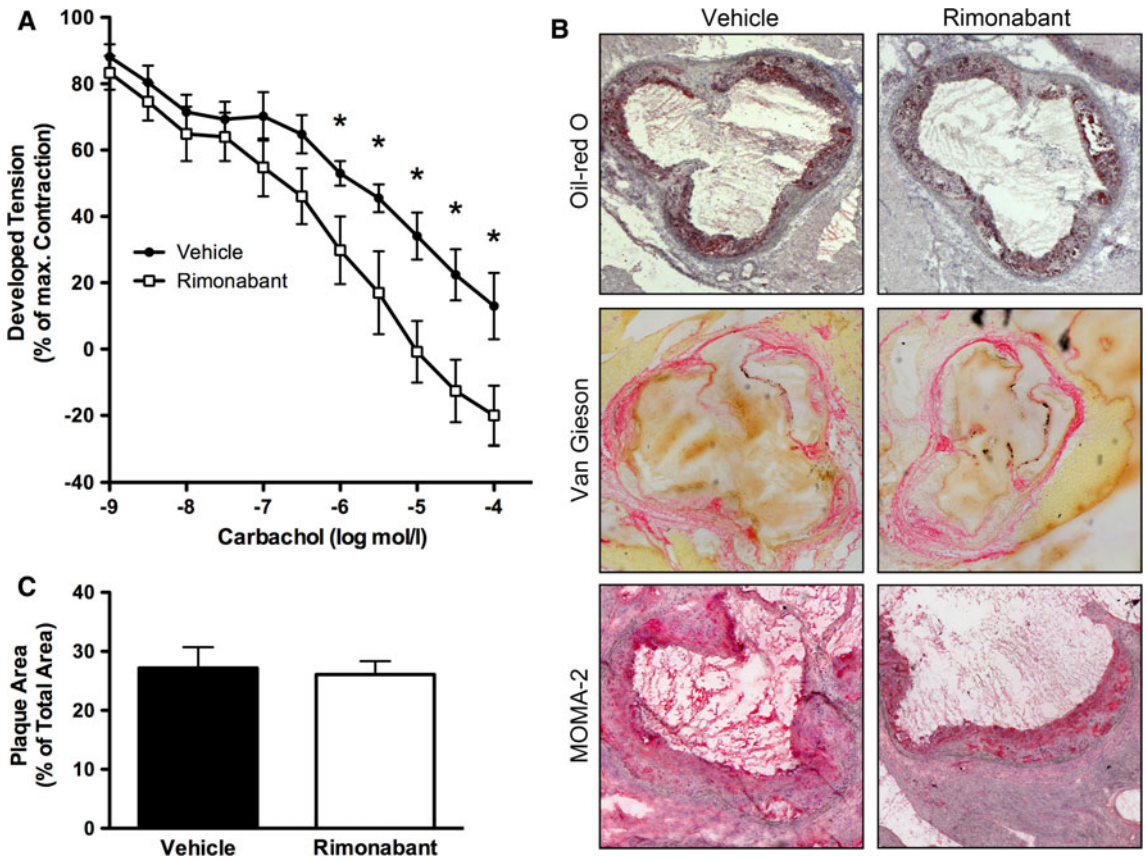

Fig. 3 **a** Aortic segments of ApoE−/− mice were isolated after 7 weeks of cholesterol-rich diet and treatment with either vehicle or rimonabant. Endothelial function was assessed in organ chamber experiments. Endothelium-dependent vasodilation induced by carbachol is shown. Mean ± SEM, $n = 10$, $^*p < 0.05$ versus vehicle. **b** Representative histological cross-sections of the aortic root stained with oil red O, van Gieson and MOMA-2 to display atherosclerotic plaque development, collagen content and macrophage infiltration. **c** Quantitative analysis of atherosclerotic lesion formation indicated as plaque area in % of total area. Mean ± SEM, $n = 10$

control, $p < 0.05$; rimonabant: 46 ± 6% of control, $p < 0.05$; Ang II and rimonabant: 46 ± 13% of control, $p < 0.05$, Fig. 5a). This interaction between CB_1-R inhibition and the AT1-R might be responsible for the reduced ROS production, but to exclude other contributing factors, we additionally investigated rac1 and manganese superoxide dismutase (MnSOD) protein expression. Neither rac1, the activating cytosolic subunit of the NADPH oxidase, nor the antioxidant enzyme MnSOD was affected by CB_1-R inhibition (data not shown). To investigate whether AT1-R down-regulation is directly controlled by the CB_1-R, we incubated VSMC with the synthetic CB_1-R antagonist AM251 (a biarylpyrazole structurally very close to rimonabant, only the *p*-chloro group attached to the phenyl substituent at C-5 of the pyrazole ring is replaced with a *p*-iodo group) and the competitive CB_1-R agonist CP 55,940. Like rimonabant, AM251 led to significant down-regulation of the AT1-R. CP 55,940 on the other hand, caused an up-regulation of the AT1-R. Co-incubation of CP 55,940 with rimonabant abolished rimonabant-induced AT1-R down-regulation (rimonabant: 37 ± 16% of control, $p < 0.05$ vs. control; AM251: 74 ± 6% of control, $p < 0.05$ vs. control; CP 55,940: 169 ± 26% of control, $p < 0.05$ vs. control; rimonabant and CP 55,940: 136 ± 16% of control, $p < 0.05$ vs. rimonabant, Fig. 5b). To confirm the effect of CB_1-R inhibition on AT1-R expression found in rat aortic VSMCs in murine cells, we performed additional experiments in cultured mouse aortic VSMCs. Consistently, stimulation with rimonabant led to a significant down-regulation of AT1-R mRNA expression compared to control in these cells (data not shown), indicating that the observed effect is not rat-specific. Together, these results suggest that down-regulation of the AT1-R by rimonabant is regulated by CB_1-R activity.

To evaluate whether AT1-R expression is also affected by CB_1-R inhibition in vivo, we next studied AT1-R expression in the aortic wall of ApoE−/− mice that received cholesterol-rich diet and rimonabant for 7 weeks. Consistent with the in vitro findings, both AT1-R protein

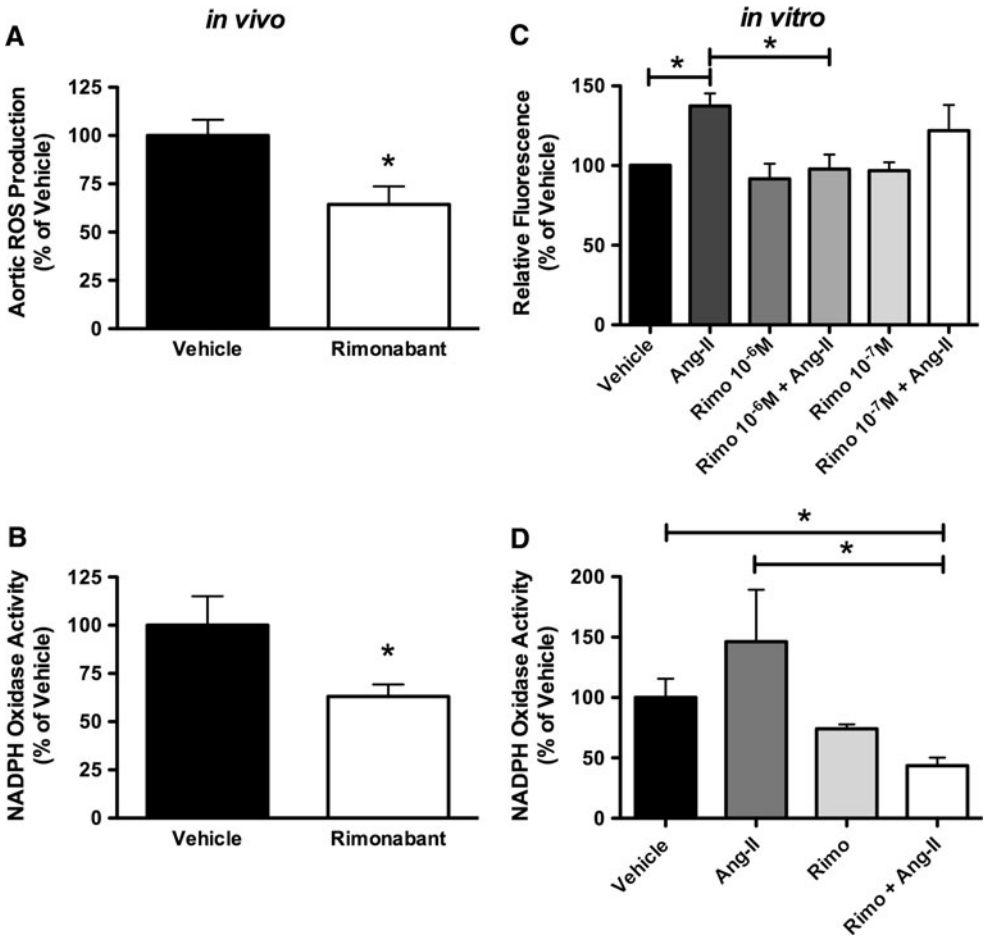

Fig. 4 ROS production and NADPH oxidase activity in isolated aortic segments of vehicle and rimonabant-treated ApoE−/− mice after 7 weeks of cholesterol-rich diet. **a** Relative vascular ROS formation was assessed by L-012 chemiluminescence. Mean ± SEM, $n = 8$, $^*p < 0.05$ versus vehicle. **b** Lucigenin-enhanced chemiluminescence assays were used to assess vascular NADPH oxidase activity. Mean ± SEM, $n = 8$, $^*p < 0.05$ versus vehicle. **c** Cultured rat aortic VSMCs were incubated with vehicle, rimonabant (10^{-6} or 10^{-7} M) for 24 h, angiotensin II for 3 h, or a combination of rimonabant and angiotensin II. Intracellular ROS production was visualized by DCF fluorescence microscopy. Mean ± SEM, $n = 4$, $^*p < 0.05$. **d** Lucigenin-enhanced chemiluminescence assays were used to assess NADPH oxidase activity in cultured rat aortic VSMCs incubated with vehicle, rimonabant for 24 h, angiotensin II for 3 h, or a combination of rimonabant and angiotensin II. Mean ± SEM, $n = 4$, $^*p < 0.05$

(24 ± 3% of control, $p < 0.05$, Fig. 5c, left) and mRNA (control: 1.0 ± 0.03 $2^{-\Delta\Delta Ct}$; rimonabant: 0.49 ± 0.13 $2^{-\Delta\Delta Ct}$, $p < 0.05$, Fig. 5c, right) levels were significantly decreased in mice that received rimonabant treatment.

CB_2 receptor inhibition and AT1 receptor expression

A functional interaction between CB_1 and CB_2 receptors has been postulated previously. We, therefore, studied CB_2-R expression in cultured aortic VSMC of C57Bl6 mice and Sprague Dawley rats, but did not detect CB_2 receptor protein (Western analysis) or mRNA (real-time RT-PCR) under basal conditions (data not shown). Furthermore, CB_2-R mRNA and protein expression were still not detectable after incubation with rimonabant, AM251, CP 55,940 or the specific CB_2-R antagonist SR 144528 (data not shown). Nevertheless, to further study the interplay between the endocannabinoid system and AT1-R expression, we analyzed AT1-R expression after CB_2-R inhibition with SR 144528. There was no change in AT1-R expression after CB2-R inhibition on both mRNA (vehicle: 1.0 ± 0.23 $2^{-\Delta\Delta Ct}$; SR 144528: 1.17 ± 0.21 $2^{-\Delta\Delta Ct}$, Fig. 5d, right) and protein level (vehicle: 100 ± 8.7%; SR 144528: 82.4 ± 11.1%, Fig. 5d, left).

Discussion

The data presented in this study confirm that the CB_1-R is expressed in rat and mouse aortic VSMCs and in aortic tissue of mice and demonstrate that oral administration of the selective CB_1-R antagonist rimonabant has atheroprotective effects by down-regulation of the AT1 receptor, reduced NADPH oxidase activity, decreased vascular

oxidative stress and thus improved endothelial function in hypercholesterolemic ApoE−/− mice.

Large clinical trials with rimonabant have shown significant improvements in cardio-metabolic risk factors including waist circumference, systolic blood pressure, HDL-cholesterol, triglyceride levels and insulin sensitivity [11, 35, 39, 48]. Because these risk factors are associated with the development of atherosclerosis [18], it was proposed that rimonabant may be beneficial in preventing or protracting atherogenesis. However, the results of the recent STRADIVARIUS trial that evaluated the effect of rimonabant treatment on the progression of coronary atherosclerosis were inconclusive [32]. The aim of the presented study was, therefore, to analyze the metabolic and vascular effects of rimonabant in a mouse model of atherosclerosis and to investigate the underlying molecular mechanisms involved.

The mouse model of atherosclerosis used in our study (ApoE−/−) has been described in numerous publications and is well-established [5, 14, 33]. When apolipoprotein E is absent or has binding defects, atherosclerotic plaques and endothelial dysfunction may develop. When homozygous animals are fed with a high-fat and cholesterol-rich diet, plasma cholesterol levels increase several fold compared to wild-type and heterozygous animals. The main finding in the model of ApoE−/− mice is that these animals develop spontaneous atherosclerotic lesions even when on a normal diet. When ApoE−/− mice were treated for 4 weeks with a high-fat diet, plasma cholesterol levels and atherosclerotic lesion area were three times higher than in ApoE−/− mice on a normal diet. Between 5–6 weeks of age, monocytes begin to adhere to endothelial cells, lipids begin to interact with matrix filaments and lipid particles begin to aggregate. It is well known that apolipoprotein E exerts anti-atherosclerotic effects by its antioxidant, anti-proliferative, anti-inflammatory, anti-platelet and NO protecting properties [5, 14, 33].

Several studies have shown the proinflammatory status of ApoE−/− mice. Judkins et al. [20] demonstrated increased superoxide production, reduced nitric oxide bioavailability and an early atherosclerotic plaque formation. We have previously shown that ApoE−/− mice display significantly higher levels of aortic superoxide production [51]. Continuous treatment with rimonabant over the entire course of the diet led to a marked improvement of endothelial function, but was not sufficient to significantly alter atherosclerotic plaque formation, collagen content or macrophage infiltration. The combined effect of apolipoprotein E deficiency and cholesterol challenge may have been too great of a burden to be sufficiently inhibited by CB_1 receptor antagonism in our experimental setting. This may be due to the duration, timing and dosage of the treatment. Recently, Dol-Gleizes et al. [13] demonstrated that rimonabant treatment of LDL-R−/− mice resulted in a dose-dependent inhibition of atherosclerotic lesions and inflammation. Their study differed in three main aspects from our investigation. First, the model of LDL receptor knockout mice was used which differs from the model of ApoE−/− mice used in our study. Second, fivefold higher rimonabant doses were used (50 mg/kg/day rimonabant for the most pronounced effects vs. 10 mg/kg/day in our study). Third, mice were treated for 3 months as compared to 7 weeks in our study. Nevertheless, the data from our study demonstrate vasculoprotective effects with the rimonabant dose used.

Wild-type mice and especially ApoE−/− mice that receive a high-fat, cholesterol-rich diet are known to gain body weight due to increased adipose tissue within days to weeks [5]. Treatment with rimonabant in a diet-induced obesity mouse model modulates food intake and thus results in moderate weight loss [7, 12, 36, 56]. Interestingly, we registered a slight increase in body weight in both the rimonabant and vehicle-treated groups although abdominal fatty tissue decreased in the rimonabant group. This effect is probably due to a weight redistribution and/or different metabolism of serum glucose [57], but further analysis is required to reveal the underlying mechanisms. Thus far, it is known that glucose uptake by muscle and brown adipose tissue is improved in mice lacking ApoE when fed a diabetogenic diet [19]. The improved insulin sensitivity observed in our rimonabant-treated animals may have caused better muscle metabolism and thus increased muscle mass.

In general, ApoE−/− mice exhibit lower body weight and insulin levels than ApoE+/+ mice when fed a diabetogenic diet [19]. Furthermore, insulin sensitivity and fasting glucose levels are age-dependent [16, 19]. We found significant differences between 9-month-old and 12-week-old ApoE−/− mice. Rimonabant treatment improved insulin sensitivity only in the older mice. It is known that CB_1-R−/− mice have lower plasma insulin levels and do not develop diet-induced insulin resistance [37]. The inhibition of CB_1 receptors via rimonabant may prevent the impaired insulin sensitivity induced by high-energy feeding observed in wild-type animals. This finding may be related to the low adiposity of rimonabant-treated mice fed the high-energy diet, as insulin sensitivity was shown to correlate with the level of fat storage [22, 41].

ROS such as superoxide are involved in the pathogenesis of atherosclerosis, and the NADPH oxidase is one major source of ROS formation in vascular cells [17, 50]. An important effect of AT1 receptor stimulation by angiotensin II is the activation of NADPH oxidase [30, 31]. In conjunction with this, our findings show that rimonabant reduces angiotensin II-mediated NADPH oxidase activity in vivo and in vitro. Importantly, we demonstrate that

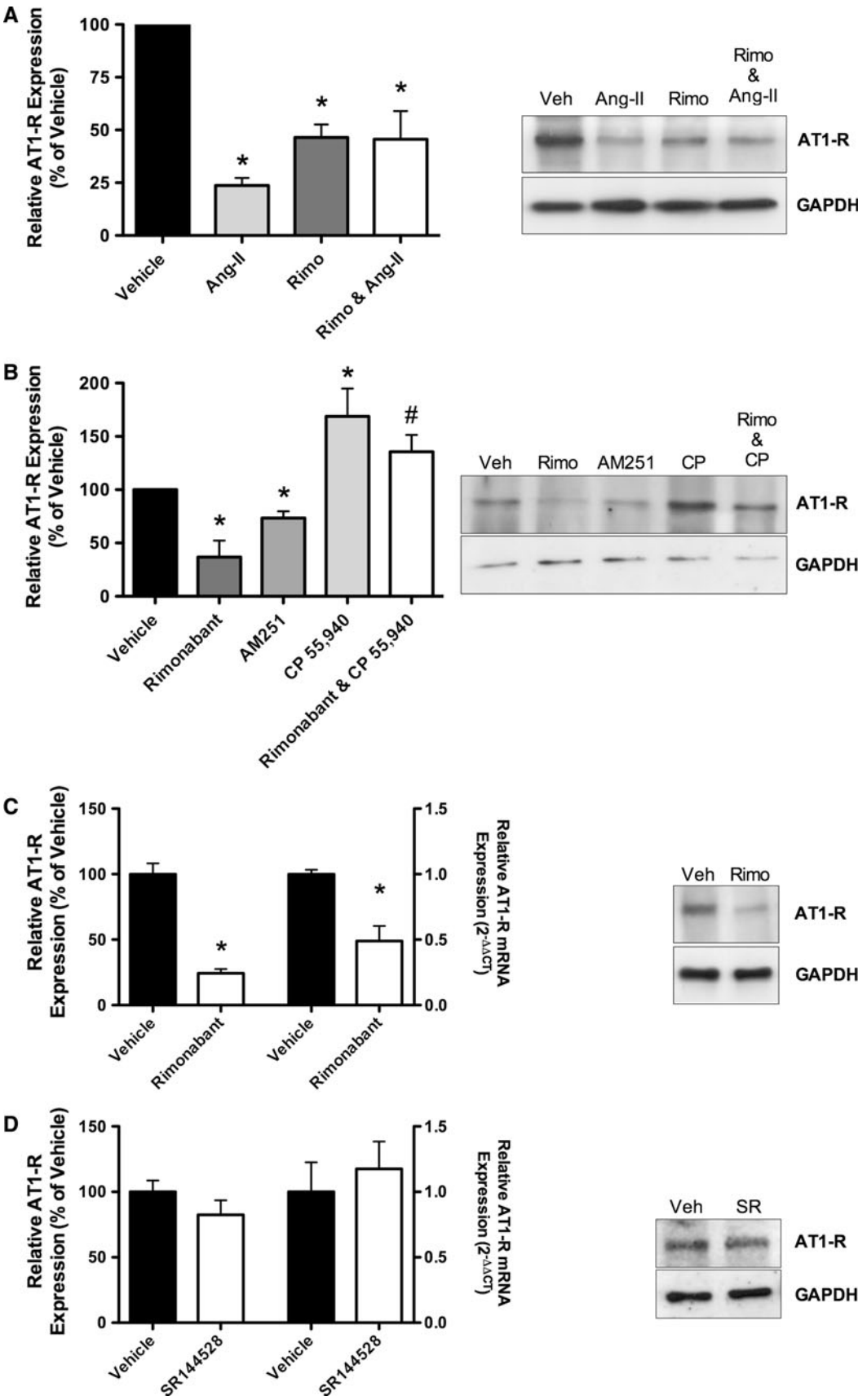
A
Relative AT1-R Expression (% of Vehicle)
100
75
50
25
0
Vehicle
Ang-II
Rimo
Rimo & Ang-II
Veh
Ang-II
Rimo
Rimo & Ang-II
AT1-R
GAPDH
B
Relative AT1-R Expression (% of Vehicle)
200
150
100
50
0
Vehicle
Rimonabant
AM251
CP 55,940
Rimonabant & CP 55,940
Veh
Rimo
AM251
CP
Rimo & CP
AT1-R
GAPDH
C
Relative AT1-R Expression (% of Vehicle)
Relative AT1-R mRNA Expression (2-ΔΔCT)
150
100
50
0
1.5
1.0
0.5
0.0
Vehicle
Rimonabant
Vehicle
Rimonabant
Veh
Rimo
AT1-R
GAPDH
D
Relative AT1-R Expression (% of Vehicle)
Relative AT1-R mRNA Expression (2-ΔΔCT)
150
100
50
0
1.5
1.0
0.5
0.0
Vehicle
SR144528
Vehicle
SR144528
Veh
SR
AT1-R
GAPDH

◀ **Fig. 5** **a** AT_1 receptor protein expression was assessed by Western blot in rat aortic VSMCs stimulated with vehicle, angiotensin II (3 h) or rimonabant (24 h). GAPDH served as loading control. Representative blot and quantitative analysis. Mean ± SEM, $n = 6$, $^*p < 0.05$ versus vehicle. **b** AT_1 receptor protein expression was assessed by Western blot in rat aortic VSMCs stimulated with vehicle, rimonabant (24 h), the CB_1-R antagonist AM251 (24 h) or the CB_1-R agonist CP 55,940 (24 h). GAPDH served as loading control. Representative blot and quantitative analysis. Mean ± SEM, $n = 4$, $^*p < 0.05$ versus vehicle, $^{\#}p < 0.05$ versus rimonabant. **c** (*left*) AT_1 receptor protein expression was assessed by Western blot in aortic homogenates of ApoE−/− mice treated concomitantly with cholesterol-rich diet and rimonabant or vehicle. GAPDH served as loading control. Representative blot and quantitative analysis. Mean ± SEM, $n = 5$, $^*p < 0.05$ versus vehicle. **c** (*right*) AT_1 receptor mRNA expression was assessed by real-time RT-PCR in aortic homogenates of the aforementioned mice. Quantitative analysis. Mean ± SEM, $n = 5$, $^*p < 0.05$ versus vehicle. **d** AT_1 receptor protein (*left*) and mRNA (*right*) expression was assessed in rat aortic VSMCs after incubation with vehicle or the CB_2-R antagonist SR 144528 for 24 h. Mean ± SEM, $n = 5$

rimonabant decreases AT1 receptor expression in the aortic wall and cultured VSMCs. It may be speculated that rimonabant leads to improved endothelial function by down-regulation of the AT1 receptor and thus decreased vascular oxidative stress. Other studies have also shown interactions between AT1 receptor and CB_1 receptor functions. Turu et al. [47] recently highlighted that the CB_1 receptor is activated following AT1 receptor stimulation. To exclude other relevant mechanisms affected by CB1-R inhibition, we analyzed rac1 and MnSOD. Physiologically, both are involved in generation and inactivation, respectively of ROS and oxidative stress [21, 55]. Neither rac1 nor MnSOD protein expression was modified by CB_1 inhibition.

Interaction between the endocannabinoid system and atherosclerosis is not only attributed to the CB_1 receptor, but the CB_2 receptor is also involved. Steffens et al. [43] have demonstrated that low dose oral cannabinoid therapy reduces atherosclerosis via the CB_2 receptor in ApoE−/− mice. One can speculate that CB_1 receptor antagonism may lead to increased endocannabinoid levels via a negative feedback mechanism. These endocannabinoids could then stimulate the CB_2 receptor and thus attenuate atherosclerosis. The precise cells and pathways involved in this CB_2-R-mediated atheroprotection are not known, but the immuno-modulatory actions of CB_2-R stimulation are currently a prime target [27]. Our data suggest that in contrast to the CB_1-R, the CB_2-R is not expressed in VSMCs under basal conditions and does not have a direct effect on AT1-R expression in these cells in an in vitro setting. However, this does not exclude a systemic interplay between CB_2-R action and aortic cells in vivo.

Several signaling pathways are involved and have been described after activation of CB_1-R [10, 29]. CB_1-R activation modulates adenylate cyclase activity in most tissues and regulates calcium and potassium channels [46]. Recent evidence suggests that cannabinoids can activate mitogen-activated protein kinases (MAPK), e.g., p42/p44 MAPK, p38 MAPK and c-Jun N-terminal kinase (JNK) through specific phosphorylation [46]. These signaling pathways play an important role and have an impact on cardiac and vascular function [40, 45]. Recently, Sugamura et al. demonstrated a greater CB_1-R expression in lipid-rich atherosclerotic plaques compared to fibrous plaques. Interestingly, they showed after CB_1-R antagonism, a significant increase in cytosolic cAMP levels, inhibited phosphorylation of c-Jun N-terminal kinase and a significant decrease in the production of proinflammatory mediators such as IL1β, IL6, IL8, TNF alpha and MMP-9 in macrophages. The authors summarized a benefit for the progression of atherosclerosis through an anti-inflammatory process by CB_1-R blockade [44]. Liu et al. [25] alluded that CB_1-R located in endothelial cells are coupled to the MAP kinase cascade, so that this modulation is involved in cell growth and proliferation with a consecutive important role in atherosclerosis. The precise cross-link between CB1-R signal transduction and vascular function remains to be investigated in further studies.

The presented data provide an important framework for the molecular mechanisms of CB_1 receptors in the development of atherosclerosis. CB_1-R inhibition promotes AT1 receptor down-regulation, reduces NADPH oxidase activity and vascular ROS burden, and improves endothelial function in vivo, indicating beneficial direct vascular effects.

Acknowledgments This study was supported by the Deutsche Forschungsgemeinschaft (DFG) and by an unrestricted research grant from Sanofi-Aventis. The excellent technical assistance of Isabel Paez-Maletz, Annika Bohner, Kathrin Paul, Susanne Schnell and Anja Kerksiek is greatly appreciated.

References

1. Baumer AT, Wassmann S, Ahlbory K, Strehlow K, Muller C, Sauer H, Bohm M, Nickenig G (2001) Reduction of oxidative stress and AT1 receptor expression by the selective oestrogen receptor modulator idoxifene. Br J Pharmacol 134:579–584
2. Begg M, Pacher P, Batkai S, Osei-Hyiaman D, Offertaler L, Mo FM, Liu J, Kunos G (2005) Evidence for novel cannabinoid receptors. Pharmacol Ther 106:133–145
3. Bensaid M, Gary-Bobo M, Esclangon A, Maffrand JP, Le Fur G, Oury-Donat F, Soubrie P (2003) The cannabinoid CB1 receptor antagonist SR141716 increases Acrp30 mRNA expression in adipose tissue of obese fa/fa rats and in cultured adipocyte cells. Mol Pharmacol 63:908–914
4. Buckley NE, McCoy KL, Mezey E, Bonner T, Zimmer A, Felder CC, Glass M (2000) Immunomodulation by cannabinoids is absent in mice deficient for the cannabinoid CB(2) receptor. Eur J Pharmacol 396:141–149
5. Calleja L, Paris MA, Paul A, Vilella E, Joven J, Jimenez A, Beltran G, Uceda M, Maeda N, Osada J (1999) Low-cholesterol and high-fat diets reduce atherosclerotic lesion development in

ApoE-knockout mice. Arterioscler Thromb Vasc Biol 19:2368–2375
6. Colombo G, Agabio R, Diaz G, Lobina C, Reali R, Gessa GL (1998) Appetite suppression and weight loss after the cannabinoid antagonist SR 141716. Life Sci 63:L113–L117
7. Cota D, Marsicano G, Lutz B, Vicennati V, Stalla GK, Pasquali R, Pagotto U (2003) Endogenous cannabinoid system as a modulator of food intake. Int J Obes Relat Metab Disord 27:289–301
8. Croci T, Manara L, Aureggi G, Guagnini F, Rinaldi-Carmona M, Maffrand JP, Le Fur G, Mukenge S, Ferla G (1998) In vitro functional evidence of neuronal cannabinoid CB1 receptors in human ileum. Br J Pharmacol 125:1393–1395
9. De Petrocellis L, Cascio MG, Di Marzo V (2004) The endocannabinoid system: a general view and latest additions. Br J Pharmacol 141:765–774
10. Demuth DG, Molleman A (2006) Cannabinoid signalling. Life Sci 78:549–563
11. Despres JP, Golay A, Sjostrom L (2005) Effects of rimonabant on metabolic risk factors in overweight patients with dyslipidemia. N Engl J Med 353:2121–2134
12. Di Marzo V, Matias I (2005) Endocannabinoid control of food intake and energy balance. Nat Neurosci 8:585–589
13. Dol-Gleizes F, Paumelle R, Visentin V, Mares AM, Desitter P, Hennuyer N, Gilde A, Staels B, Schaeffer P, Bono F (2008) Rimonabant, a selective cannabinoid CB1 receptor antagonist, inhibits atherosclerosis in LDL receptor-deficient mice. Arterioscler Thromb Vasc Biol 29:12–18
14. Ferre N, Camps J, Paul A, Cabre M, Calleja L, Osada J, Joven J (2001) Effects of high-fat, low-cholesterol diets on hepatic lipid peroxidation and antioxidants in apolipoprotein E-deficient mice. Mol Cell Biochem 218:165–169
15. Gadde KM, Allison DB (2006) Cannabinoid-1 receptor antagonist, rimonabant, for management of obesity and related risks. Circulation 114:974–984
16. Gao J, Katagiri H, Ishigaki Y, Yamada T, Ogihara T, Imai J, Uno K, Hasegawa Y, Kanzaki M, Yamamoto TT, Ishibashi S, Oka Y (2007) Involvement of apolipoprotein E in excess fat accumulation and insulin resistance. Diabetes 56:24–33
17. Harrison DG, Cai H, Landmesser U, Griendling KK (2003) Interactions of angiotensin II with NAD(P)H oxidase, oxidant stress and cardiovascular disease. J Renin Angiotensin Aldosterone Syst 4:51–61
18. Heusch G (2006) Obesity—a risk factor or a RISK factor for myocardial infarction? Br J Pharmacol 149:1–3
19. Hofmann SM, Perez-Tilve D, Greer TM, Coburn BA, Grant E, Basford JE, Tschop MH, Hui DY (2008) Defective lipid delivery modulates glucose tolerance and metabolic response to diet in apolipoprotein E-deficient mice. Diabetes 57:5–12
20. Judkins CP, Diep H, Broughton BR, Mast AE, Hooker EU, Miller AA, Selemidis S, Sobey CG, Dusting GJ, Drummond GR (2010) Direct evidence of a role for Nox2 in superoxide production, reduced nitric oxide bioavailability and early atherosclerotic plaque formation in ApoE−/− mice. Am J Physiol Heart Circ Physiol 298:H24–H32
21. Khanday FA, Yamamori T, Mattagajasingh I, Zhang Z, Bugayenko A, Naqvi A, Santhanam L, Nabi N, Kasuno K, Day BW, Irani K (2006) Rac1 leads to phosphorylation-dependent increase in stability of the p66shc adaptor protein: role in Rac1-induced oxidative stress. Mol Biol Cell 17:122–129
22. Kim JY, Nolte LA, Hansen PA, Han DH, Ferguson K, Thompson PA, Holloszy JO (2000) High-fat diet-induced muscle insulin resistance: relationship to visceral fat mass. Am J Physiol Regul Integr Comp Physiol 279:R2057–R2065
23. Klein TW, Newton C, Larsen K, Lu L, Perkins I, Nong L, Friedman H (2003) The cannabinoid system and immune modulation. J Leukoc Biol 74:486–496
24. Lim SY, Davidson SM, Yellon DM, Smith CC (2009) The cannabinoid CB1 receptor antagonist, rimonabant, protects against acute myocardial infarction. Basic Res Cardiol 104:781–792
25. Liu J, Gao B, Mirshahi F, Sanyal AJ, Khanolkar AD, Makriyannis A, Kunos G (2000) Functional CB1 cannabinoid receptors in human vascular endothelial cells. Biochem J 346(Pt 3):835–840
26. Livak KJ, Schmittgen TD (2001) Analysis of relative gene expression data using real-time quantitative PCR and the 2(−Delta Delta C(T)) method. Methods 25:402–408
27. Mach F, Steffens S (2008) The role of the endocannabinoid system in atherosclerosis. J Neuroendocrinol 20(Suppl 1):53–57
28. Matsuda LA, Lolait SJ, Brownstein MJ, Young AC, Bonner TI (1990) Structure of a cannabinoid receptor and functional expression of the cloned cDNA. Nature 346:561–564
29. McAllister SD, Glass M (2002) CB(1) and CB(2) receptor-mediated signalling: a focus on endocannabinoids. Prostaglandins Leukot Essent Fatty Acids 66:161–171
30. Nickenig G, Harrison DG (2002) The AT(1)-type angiotensin receptor in oxidative stress and atherogenesis. Part I. Oxidative stress and atherogenesis. Circulation 105:393–396
31. Nickenig G, Harrison DG (2002) The AT(1)-type angiotensin receptor in oxidative stress and atherogenesis. Part II. AT(1) receptor regulation. Circulation 105:530–536
32. Nissen SE, Nicholls SJ, Wolski K, Rodes-Cabau J, Cannon CP, Deanfield JE, Despres JP, Kastelein JJ, Steinhubl SR, Kapadia S, Yasin M, Ruzyllo W, Gaudin C, Job B, Hu B, Bhatt DL, Lincoff AM, Tuzcu EM (2008) Effect of rimonabant on progression of atherosclerosis in patients with abdominal obesity and coronary artery disease: the STRADIVARIUS randomized controlled trial. JAMA 299:1547–1560
33. Osada J, Joven J, Maeda N (2000) The value of apolipoprotein E knockout mice for studying the effects of dietary fat and cholesterol on atherogenesis. Curr Opin Lipidol 11:25–29
34. Pacher P, Batkai S, Kunos G (2006) The endocannabinoid system as an emerging target of pharmacotherapy. Pharmacol Rev 58:389–462
35. Pi-Sunyer FX, Aronne LJ, Heshmati HM, Devin J, Rosenstock J (2006) Effect of rimonabant, a cannabinoid-1 receptor blocker, on weight and cardiometabolic risk factors in overweight or obese patients: RIO-North America: a randomized controlled trial. JAMA 295:761–775
36. Ravinet TC, Arnone M, Delgorge C, Gonalons N, Keane P, Maffrand JP, Soubrie P (2003) Anti-obesity effect of SR141716, a CB1 receptor antagonist, in diet-induced obese mice. Am J Physiol Regul Integr Comp Physiol 284:R345–R353
37. Ravinet TC, Delgorge C, Menet C, Arnone M, Soubrie P (2004) CB1 cannabinoid receptor knockout in mice leads to leanness, resistance to diet-induced obesity and enhanced leptin sensitivity. Int J Obes Relat Metab Disord 28:640–648
38. Saavedra LE (2007) Endocannabinoid system and cardiometabolic risk. Clin Pharmacol Ther 82:591–594
39. Scheen AJ, Finer N, Hollander P, Jensen MD, Van Gaal LF (2006) Efficacy and tolerability of rimonabant in overweight or obese patients with type 2 diabetes: a randomised controlled study. Lancet 368:1660–1672
40. Seeger FH, Sedding D, Langheinrich AC, HaendelerJ, Zeiher AM, Dimmeler S. (2009) Inhibition of the p38 MAP kinase in vivo improves number and functional activity of vasculogenic cells and reduces atherosclerotic disease progression. Basic Res Cardiol. doi:10.1007/s00395-009-0072-9
41. Sindelka G, Skrha J, Prazny M, Haas T (2002) Association of obesity, diabetes, serum lipids and blood pressure regulates insulin action. Physiol Res 51:85–91
42. Steffens S, Mach F (2006) Cannabinoid receptors in atherosclerosis. Curr Opin Lipidol 17:519–526
43. Steffens S, Veillard NR, Arnaud C, Pelli G, Burger F, Staub C, Karsak M, Zimmer A, Frossard JL, Mach F (2005) Low dose oral

cannabinoid therapy reduces progression of atherosclerosis in mice. Nature 434:782–786
44. Sugamura K, Sugiyama S, Nozaki T, Matsuzawa Y, Izumiya Y, Miyata K, Nakayama M, Kaikita K, Obata T, Takeya M, Ogawa H (2009) Activated endocannabinoid system in coronary artery disease and antiinflammatory effects of cannabinoid 1 receptor blockade on macrophages. Circulation 119:28–36
45. Sun C, Liang C, Ren Y, Zhen Y, He Z, Wang H, Tan H, Pan X, Wu Z (2009) Advanced glycation end products depress function of endothelial progenitor cells via p38 and ERK 1/2 mitogen-activated protein kinase pathways. Basic Res Cardiol 104:42–49
46. Turu G, Hunyady L (2010) Signal transduction of the CB1 cannabinoid receptor. J Mol Endocrinol 44:75–85
47. Turu G, Simon A, Gyombolai P, Szidonya L, Bagdy G, Lenkei Z, Hunyady L (2007) The role of diacylglycerol lipase in constitutive and angiotensin AT1 receptor-stimulated cannabinoid CB1 receptor activity. J Biol Chem 282:7753–7757
48. Van Gaal LF, Rissanen AM, Scheen AJ, Ziegler O, Rossner S (2005) Effects of the cannabinoid-1 receptor blocker rimonabant on weight reduction and cardiovascular risk factors in overweight patients: 1-year experience from the RIO-Europe study. Lancet 365:1389–1397
49. Van Sickle MD, Duncan M, Kingsley PJ, Mouihate A, Urbani P, Mackie K, Stella N, Makriyannis A, Piomelli D, Davison JS, Marnett LJ, Di MV, Pittman QJ, Patel KD, Sharkey KA (2005) Identification and functional characterization of brainstem cannabinoid CB2 receptors. Science 310:329–332
50. Warnholtz A, Nickenig G, Schulz E, Macharzina R, Brasen JH, Skatchkov M, Heitzer T, Stasch JP, Griendling KK, Harrison DG, Bohm M, Meinertz T, Munzel T (1999) Increased NADH-oxidase-mediated superoxide production in the early stages of atherosclerosis: evidence for involvement of the renin–angiotensin system. Circulation 99:2027–2033
51. Wassmann S, Czech T, van Eickels M, Fleming I, Bohm M, Nickenig G (2004) Inhibition of diet-induced atherosclerosis and endothelial dysfunction in apolipoprotein E/angiotensin II type 1A receptor double-knockout mice. Circulation 110:3062–3067
52. Wassmann S, Laufs U, Baumer AT, Muller K, Ahlbory K, Linz W, Itter G, Rosen R, Bohm M, Nickenig G (2001) HMG-CoA reductase inhibitors improve endothelial dysfunction in normocholesterolemic hypertension via reduced production of reactive oxygen species. Hypertension 37:1450–1457
53. Wassmann S, Laufs U, Stamenkovic D, Linz W, Stasch JP, Ahlbory K, Rosen R, Bohm M, Nickenig G (2002) Raloxifene improves endothelial dysfunction in hypertension by reduced oxidative stress and enhanced nitric oxide production. Circulation 105:2083–2091
54. Wassmann S, Stumpf M, Strehlow K, Schmid A, Schieffer B, Bohm M, Nickenig G (2004) Interleukin-6 induces oxidative stress and endothelial dysfunction by overexpression of the angiotensin II type 1 receptor. Circ Res 94:534–541
55. Wenzel P, Schuhmacher S, Kienhofer J, Muller J, Hortmann M, Oelze M, Schulz E, Treiber N, Kawamoto T, Scharffetter-Kochanek K, Munzel T, Burkle A, Bachschmid MM, Daiber A (2008) Manganese superoxide dismutase and aldehyde dehydrogenase deficiency increase mitochondrial oxidative stress and aggravate age-dependent vascular dysfunction. Cardiovasc Res 80:280–289
56. Wiley JL, Burston JJ, Leggett DC, Alekseeva OO, Razdan RK, Mahadevan A, Martin BR (2005) CB1 cannabinoid receptor-mediated modulation of food intake in mice. Br J Pharmacol 145:293–300
57. Zhang C, Park Y, Picchi A, Potter BJ (2008) Maturation-induces endothelial dysfunction via vascular inflammation in diabetic mice. Basic Res Cardiol 103:407–416
58. Zimmer A, Zimmer AM, Hohmann AG, Herkenham M, Bonner TI (1999) Increased mortality, hypoactivity, and hypoalgesia in cannabinoid CB1 receptor knockout mice. Proc Natl Acad Sci USA 96:5780–5785